JACS
JOURNAL OF THE AMERICAN CHEMICAL SOCIETY
Article
pubs.acs.org/JACS

Defining the Molecular Basis of Amyloid Inhibitors: Human Islet Amyloid Polypeptide–Insulin Interactions

Anna C. Susa,[†] Chun Wu,[†,§] Summer L. Bernstein,[†] Nicholas F. Dupuis,[†] Hui Wang,[‡] Daniel P. Raleigh,[‡] Joan-Emma Shea,[†] and Michael T. Bowers*[,†]

[†]Department of Chemistry and Biochemistry, University of California, Santa Barbara, California 93106, United States
[‡]Department of Chemistry, Stony Brook University, Stony Brook, New York 11794-3400, United States

Supporting Information

ABSTRACT: Human islet amyloid polypeptide (hIAPP or Amylin) is a 37 residue hormone that is cosecreted with insulin from the pancreatic islets. The aggregation of hIAPP plays a role in the progression of type 2 diabetes and contributes to the failure of islet cell grafts. Despite considerable effort, little is known about the mode of action of IAPP amyloid inhibitors, and this has limited rational drug design. Insulin is one of the most potent inhibitors of hIAPP fibril formation, but its inhibition mechanism is not understood. In this study, the aggregation of mixtures of hIAPP with insulin, as well as with the separate A and B chains of insulin, were characterized using ion mobility spectrometry-based mass spectrometry and atomic force microscopy. Insulin and the insulin B chain target the hIAPP monomer in its compact isoform and shift the equilibrium away from its extended isoform, an aggregation-prone conformation, and thus inhibit hIAPP from forming β-sheets and subsequently amyloid fibrils. All-atom molecular modeling supports these conclusions.

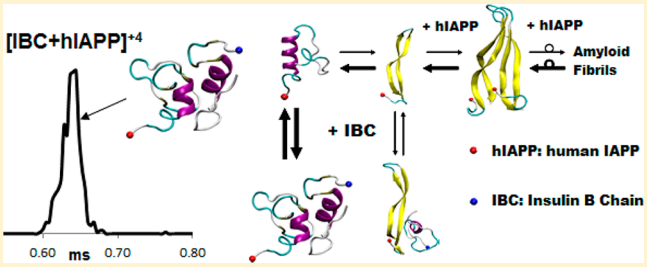

INTRODUCTION

Type 2 diabetes (T2D) is a complex disease that is reaching epidemic proportions in the developed world.[1] Affected individuals develop insulin resistance and progression of the disease is associated with a loss of β-cell mass. Human islet amyloid polypeptide (hIAPP, also known as amylin) forms islet amyloid in T2D. Evidence is increasing that soluble oligomers of hIAPP are involved in important aspects of T2D,[2−4] including β-cell death,[3,5,6] and contribute to the failure of islet graft transplants.[7−9] Thus, islet amyloid, or the process of its formation, plays a crucial role in the pathology of the disease.[10] While the mechanism of hIAPP induced β-cell toxicity is not fully understood, a range of mechanisms have been proposed and are likely to be involved in vivo. These include receptor mediated mechanisms, the triggering of localized inflammatory response and possibly IAPP induced membrane damage as well as other mechanisms.[10−14]

In contrast, monomer hIAPP is soluble and functions as a partner to insulin in glucose regulation in healthy individuals.[15] Insulin and IAPP are coregulated at the expression level, with both genes having a common promoter.[16] In healthy β-cells IAPP:insulin levels are maintained at about 1:100; however, in T2D patients this ratio can increase to 1:20.[17] Both IAPP and insulin share the same secretory pathway in the β-cells and thus have ample opportunity to interact. In the secretory granule, insulin crystallizes into the form of hexamer aggregates stabilized by two Zn^{2+} ions.[18,19] Typically these crystals occupy 50−90% of the granule volume at an effective concentration of ~40 mM and form the dense core of the granule. The remaining granule contents, including hIAPP, occupy the halo region of the granule peripheral to the dense core. Hence, in healthy β-cells hIAPP has an intragranule concentration of 0.8−4.0 mM. In vitro studies have shown that hIAPP rapidly forms fibrils at a concentration 2 orders of magnitude less than this.[20,21] In vitro cell toxicity studies further show that hIAPP oligomers induce apoptosis of pancreatic β-cells.[22] Hence, hIAPP aggregation and its cell toxicity are somehow inhibited in vivo, since hIAPP plaques are not readily detectable in nondiabetic individuals.[10] The lower pH of the granule likely plays a role, but cannot account for the high solubility of hIAPP in the intra granule environment.[23] Zn(II)-hIAPP interaction may stabilize the compact soluble hIAPP monomer.[24] Another obvious potential inhibitor is the dominant secretory pathway species, insulin. Several studies have shown insulin to be one of the most potent inhibitors of hIAPP fibrillization in vitro.[20,21,25−30] However, little is known about the mechanism of this crucial inhibition process, and it is not known if insulin and other protein-based inhibitors target the same conformation as small molecule inhibitors of hIAPP amyloid formation. One proposal is that insulin interacts with the growing hIAPP fibril tip in some unknown fashion.[20] Additional support for insulin interacting with hIAPP fibrils comes from observations that insulin interacted with preformed hIAPP fibrils attached to plasmon resonance chips.[27] Using either nonamyloidogenic rat IAPP (rIAPP)[31] or IAPP linked to a maltose binding protein,[32]

Received: April 22, 2014
Published: August 21, 2014

   dx.doi.org/10.1021/ja504031d | J. Am. Chem. Soc. 2014, 136, 12912−12919

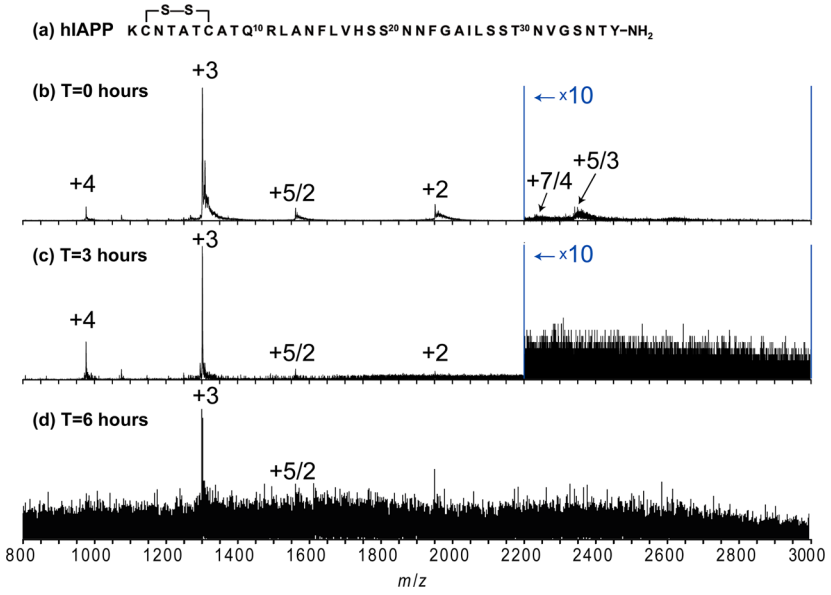

Figure 1. Sequence of hIAPP (a) and mass spectra for 20 μM hIAPP at pH 7.4 obtained at 0 (b), 3 (c) and 6 h (d) after sample preparation. Visible aggregates appeared in the sample solution after 6 h.

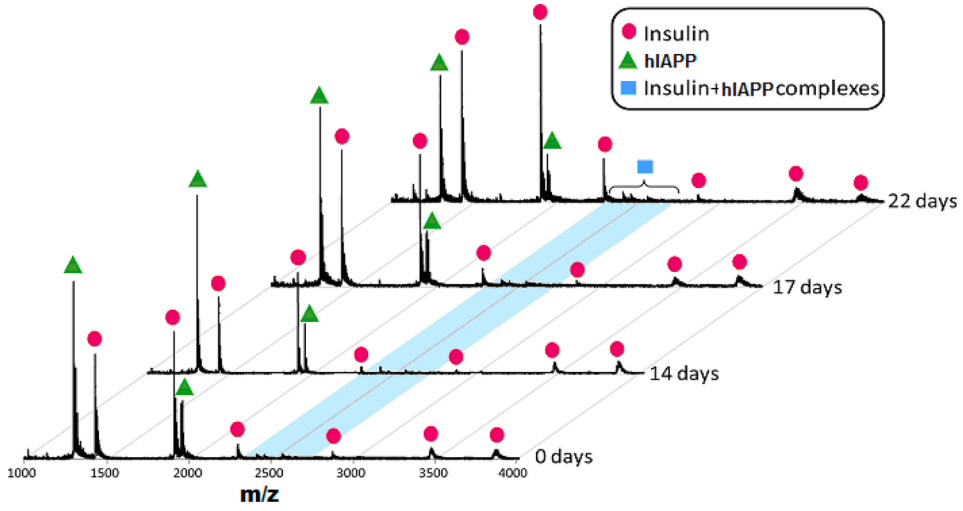

Figure 2. Mass spectra of 1:1 mixture of 20 μM hIAPP and 20 μM insulin at pH 7.4 monitored over a period of 22 days. The mixed hIAPP and insulin complexes are labeled with blue squares. The intensity of the hIAPP monomer peaks (green triangles) with respect to the insulin monomers (red dots) start to diminish between 17 and 22 days. By the 24th day, the overall intensity of the spectrum had decreased significantly.

a helix–helix interaction between the helical insulin and the N-terminal helix of IAPP was suggested to be involved in the insulin inhibition mechanism. Peptide array mapping studies have suggested potential interactions between IAPP and insulin in regions that are known to transiently form helix.[26]

We have previously used ion mobility-based mass spectrometry (IMS-MS) coupled with all-atom molecular dynamics (MD) simulations to characterize monomers[33] and dimers[34] of human IAPP and rIAPP. We showed that monomeric hIAPP can adopt multiple conformations in solution, with the two dominant ones being a helix–coil isoform and an extended β-hairpin isoform.[33] The relative abundance of these two conformers is strongly dependent on solution pH with helix–coil dominating in neutral and acidic solutions and the β-hairpin isoform dominating in basic solution. Of relevance is the fact that rIAPP does not induce β-cell apoptosis[22] and has much lower tendency to fibrillize in comparison with hIAPP.[35,36] As a consequence, we used rIAPP as a negative control[34] to help identify crucial aspects of hIAPP that lead to amyloid and possibly contribute to T2D. The rat peptide does not form amyloid under the conditions of our assays. The two peptides are identical at 31 of the 37 amino acid locations with the 6 differences occurring in the 18–29 region. Of most importance, rIAPP contains prolines at positions 25, 28, and 29 where hIAPP has Ala, Ser and Ser, and consequently rIAPP does not form amyloid, but does populate a helix–coil monomer isoform that is similar to the conformer formed by the human peptide, and a dominant compact helix–coil dimer.[34] In contrast, the cross section of the hIAPP dimer is 10% larger than the rat dimer and simulations argue that it is composed predominantly of coupled β-hairpins with a β-strand interface, suggesting that the β-hairpin form of hIAPP contributes to its early oligomer states.[34] In this conformation the β-strand interface correlates well with the binding "hot-spots" identified by Kapurniotu and co-workers through fragment binding affinity analysis.[37]

dx.doi.org/10.1021/ja504031d | J. Am. Chem. Soc. 2014, 136, 12912–12919

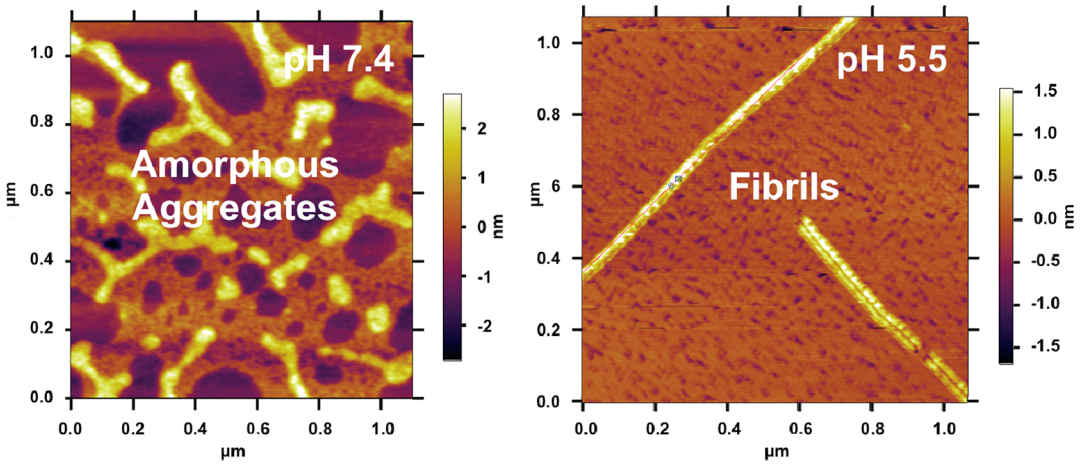

Figure 3. AFM images taken of the incubated hIAPP and insulin 20 μM mixtures. The mixture at pH 7.4 (left) after four-week incubation has no fibrils but reveals extensive amorphous aggregates. The mixture (right) at pH 5.5 after 10-day incubation reveals formation of fibrils.

Insulin is composed of a B-chain (IBC) and a smaller A-chain (IAC) connected by two disulfide bonds. Our strategy is to investigate the effects of the intact insulin molecule on hIAPP assembly and then separately study the effects of the isolated IAC and IBC fragments. The experimental studies are complemented by all atom molecular dynamics simulations in order to provide an atomistic level interpretation. The goals of this study are to provide a mechanism for the inhibition of hIAPP oligomerization by insulin, to test if insulin targets different conformations than known small molecule inhibitors, and to provide a context for beginning to develop the knowledge required for rational drug design.

RESULTS AND DISCUSSION

hIAPP Forms Amyloid but hIAPP/Insulin Mixtures Do Not. A mass spectrum of pure hIAPP (Figure 1a) at 20 μM at pH 7.4 in ammonium acetate buffer collected immediately after preparing the solution is shown in Figure 1b. The peaks are labeled by z/n, where z is the charge and n is the oligomer number. The peak near m/z = 1000 is the +4 monomer and the peak near m/z = 1310 the +3 monomer. Of interest are the oligomers that are present even at these early times; the +5/2 dimer, +5/3 trimer, 7/4 tetramer and unresolved larger oligomers near m/z = 2600. The spectra in Figure 1c,d are from the same solution but acquired 3 and 6 h later. The latter spectrum is dominated by unresolved oligomers with only a +3 monomer peak discernible. After 6 h, insoluble aggregates are visible at the bottom of the sample container.

When insulin is added forming a 1:1 hIAPP to insulin ratio at pH 7.4, very different results are obtained, and no hIAPP aggregates are detected (Figure 2). The peaks marked by (▲) are from hIAPP and those by (●) are from insulin (a spectrum of pure insulin under these conditions is provided in the Supporting Information (SI), Figure S1). The insulin peaks are exactly the same as in the pure insulin sample, showing, from low m/z to high m/z, +4 and +3 monomers, a +5/2 insulin dimer, a +2 monomer and finally +10 and +9 insulin hexamers. hIAPP, on the other hand, only shows +3 and +2 monomers, and importantly the early oligomers are absent. Little change is observed in the spectrum over the first 17 days, and only a small loss of hIAPP relative to insulin is detected by day 22. This is in stark contrast to the behavior of hIAPP by itself at the same concentration (Figure 1), where very rapid oligomer formation is observed. Finally, while no hIAPP oligomers are observed, weak heteroligomers are seen starting immediately and are designated by the (■) in the day 22 spectrum. When this region is amplified $[\text{hIAPP+insulin}]^{+4}$, $[\text{hIAPP+2insulin}]^{+5}$ and $[\text{hIAPP+3insulin}]^{+8}$ peaks are identified, but no heteroligomers with more than 1 hIAPP are detected (Figure S2 (SI)).

Insulin rapidly aggregates at pH $\leq$ 5.5, but only slowly aggregates at pH 7.4.[38,39] This behavior contrasts with hIAPP, which rapidly aggregates at high pH, but only slowly at low pH.[23] The extra-celluar environments of the islets of Langerhans (the regions of the pancreas that contain the cells which produce insulin and hIAPP) are at pH = 7.4, but the pH of secretory granule is pH 5.5.[20] Hence it is of interest to further examine the behavior of the mixture at pH 5.5 (Figure S3 (SI)). The mass spectrum of the freshly prepared sample is very similar to that of the pH 7.4 mixture (Figure 2). However, after several days, the insulin peaks disappear, then the hIAPP (+3 and +2) monomer peaks diminish in intensity. After 15 days, very little hIAPP monomer is left in solution, indicating that almost all of the insulin and hIAPP have been consumed, and insoluble aggregates are visible at the bottom of the sample container. For a sample of pure insulin at pH 5.5 under identical conditions, a similar aggregation pattern was observed (Figure S4 (SI)): the initial mass spectrum is nearly identical to the mass spectrum of an insulin sample at pH 7.4 (Figure S1 (SI)). However, after 1 day, the oligomeric peaks begin to disappear as insulin aggregates and precipitates.

In order to investigate the effects of insulin on the morphology of the insoluble aggregates, aliquots from the incubated samples were dried on freshly cleaved mica and imaged with an atomic force microscope using the protocol employed in our previous study[33] (Figure 3). In the pH 7.4 mixture, where hIAPP is soluble for up to 4 weeks, amorphous aggregates are observed, lacking the typical amyloid fiber morphology. In the pH 5.5 mixture, fibrils are observed, and their dimensions were consistent with our early finding of the hIAPP fibrils.[33] The fibrils are ~50 nm wide and have an axial periodicity of 25−40 nm, which is characteristic of the amyloid fibril twist.[40] Gazit and co-workers[26] using fluorescence assays and CD have shown that the insulin B-chain inhibits fibril formation of hIAPP, but the A-chain does not. They used peptide arrays to deduce that residues of the 9−20 B-chain (S^{9}HLVEALYLVCG^{20}) form contacts with the 7−19 sequence

dx.doi.org/10.1021/ja504031d | J. Am. Chem. Soc. 2014, 136, 12912−12919

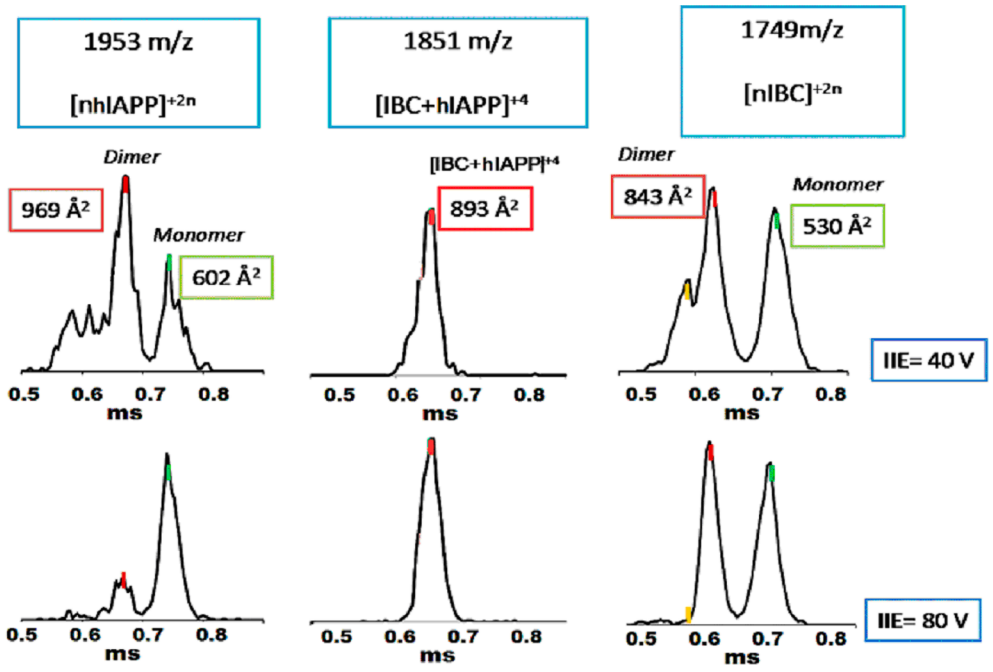

Figure 4. Arrival time distributions (ATDS) of $[nhIAPP]^{+2n}$, $[IBC+hIAPP]^{+4}$ and $[nIBC]^{+2n}$ under two ion injection voltages (40 and 80 V). At the lower injection voltage: the ATD of $[nhIAPP]^{+2n}$ shows a monomer, dimer, and smaller trimer and tetramer features; the ATD of the $[IBC+hIAPP]^{+4}$ shows mainly $[IBC+hIAPP]^{+4}$ with a cross section of 893 Å^2; and the ATD of $[nIBC]^{+2n}$ has monomer with a cross section of 530 Å^2 and dimer with a cross section of 843 Å^2 and probably a small amount of trimer at shortest times. At the higher injection voltage: the large oligomers dissociate, leaving monomer and dimer as dominant species in all cases.

of hIAPP (C^7ATQRLANFLVHS[19]). The B-chain is helical in the intact insulin molecule, and this region of hIAPP has also been shown to transiently populate helical ϕ and ψ angles in vitro at pH 7.4.[41,42] Hence, we felt it important to look at the effects of the A-chain and B-chain on early oligomer assembly of hIAPP using IMS-MS methods. Mass spectra of a mixture of 1:1 insulin A chain (IAC) with hIAPP (Figure S5 (SI)) and a mixture of 1:1 insulin B chain (IBC) with hIAPP (Figure S6 (SI)) at pH 7.4 were obtained over the course of several weeks. In the 1:1 mixture of IBC and hIAPP, a heterogeneous cluster of $[hIAPP \text{ and } IBC]^{+4}$ is observed, while no heterogeneous clusters are visible in the IAC and hIAPP mixture. Over the course of 3 weeks, the mass spectrum of the hIAPP and IBC sample remains almost the same, with only a small decrease in hIAPP observed relative to IBC. Different behavior is observed with the sample of hIAPP and IAC; the hIAPP z/n = +4, +3, +2 peaks decrease and disappear after a few days, indicating that the sample has aggregated. From these time course studies, we conclude that IBC and full-length insulin interact with hIAPP in a similar fashion: they stabilize hIAPP for several weeks, and their monomers form heterogeneous clusters with one hIAPP monomer. In contrast, IAC does not inhibit hIAPP aggregation and does not form heteroligomers with hIAPP.

The Cross Section of the IBC-hIAPP Heterodimer: An Important Modeling Constraint. Gazit and co-workers[26] showed that peptide fragments from a helical region of IBC interact with peptide fragments from the region of hIAPP that can form a transient helical structure. This suggests that a helix–helix interaction may be involved in the IBC-hIAPP interactions and insulin-hIAPP interactions that lead eventually to fibril inhibition in hIAPP. We address this point in detail using all atom modeling studies which are described in the next section. Here we obtain the cross section of the IBC-hIAPP heterodimer observed in the mass spectrum in Figure S6 (SI). This cross section will be important in defining the lower energy heterodimer structures obtained from the modeling studies.

The arrival time distribution (ATD) for the $[IBC+hIAPP]^{+4}$ heterodimer is given in the center panel of Figure 4. The ATD consists of one dominant peak centered near 0.65 ms arrival time and a weak shoulder to shorter times. This ATD is flanked on the left by the $[nhIAPP]^{+2n}$ ATD and on the right by the $[nIBC]^{+2n}$ ATD obtained from the same mass spectrum as the heterodimer. These are included to firmly identify the peak assigned as $[IBC+hIAPP]^{+4}$, as will be demonstrated. The ATDs across the top panel were obtained at a lower injection energy (see Materials and Methods section) than those in the bottom panel. As the energy is increased, the ions experience transient collisional heating that can lead to dissociation of higher oligomers into smaller species. For example, the $[nhIAPP]^{+2n}$ ATD greatly simplifies due to dissociation of higher order oligomers when the injection energy is increased to 80 V from 40 V. This allows assignment of the peak near 0.74 ms as the $hIAPP^{+2}$ monomer and the peak near 0.66 ms as the $(2\ hIAPP)^{+4}$ dimer. Similar assignments are made for the IBC^{+2} monomer and $(2\ IBC)^{+4}$ dimer. Importantly, the ATD for the $[IBC+hIAPP]^{+4}$ heterodimer remains almost unchanged at higher injection energy with only a reduction of the shorter time shoulder observed. Hence we can unambiguously make the assignments of 843 Å^2 for the $(2\ IBC)^{+4}$ dimer, 893 Å^2 for the $[IBC+hIAPP]^{+4}$ dimer and 969 Å^2 for the $(2\ hIAPP)^{+4}$ dimer, cross sections consistent with the relative increase in size of these dimers (60, 67 and 74 residues, respectively).

Insulin and the IBC Reduce the Amyloidogenic Conformer of Monomeric hIAPP. The question arises as to how IBC and insulin inhibit the hIAPP assembly process. Both peptides form heterodimers with hIAPP that are in

dx.doi.org/10.1021/ja504031d | J. Am. Chem. Soc. 2014, 136, 12912–12919

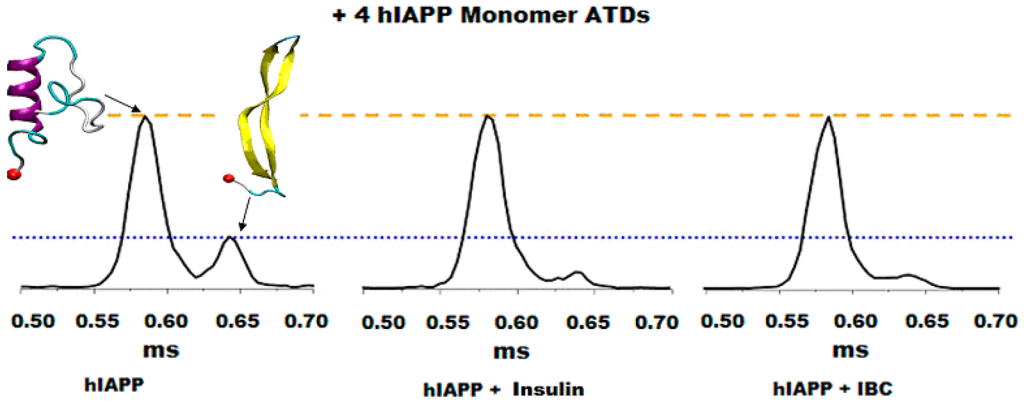

Figure 5. ATDs of the +4 hIAPP monomer. The ATD on the left is of the +4 hIAPP monomer in a solution of pure hIAPP. The +4 hIAPP monomer ATD in the middle was acquired from a sample of 1:1 mixture of hIAPP and insulin, and the ATD on the far right was from a sample of 1:1 mixture of hIAPP and IBC. The ATDs in the three samples were acquired at the same instrumental settings at ion injection energy of 40 V. The large feature on the left in the ATDs corresponds to compact α-helical structures of the +4 hIAPP monomer, while the feature on the right corresponds to an extended β-hairpin structure previously described by Dupuis et al.[24] The relative abundance of the β-hairpin feature is much smaller in the mixtures of hIAPP with insulin and IBC than it is in the sample of pure hIAPP. All samples are at concentrations of 20 μM and at pH 7.4.

dynamic equilibrium with the monomers. How does this process affect the conformer distribution of hIAPP? Using IMS-MS, ATDs of the +4 human hIAPP monomer were obtained from three samples at the same instrumental settings: a pure hIAPP sample, a sample of 1:1 hIAPP and insulin, and a sample of 1:1 hIAPP and IBC (Figure 5). The ATD of the +4 hIAPP monomer in the sample of pure hIAPP corresponds to that previously shown by Dupuis et al:[33] the feature on the left has a cross section of 653 Å^2 consistent with a helix−coil structure, and the feature on the right has a cross section of 770 Å^2 consistent with a more extended β-hairpin structure.[33]

The ATDs of the hIAPP +4 monomer in the three samples (pure hIAPP, hIAPP and IBC, hIAPP and insulin) all show these same two peaks, and the cross sections are identical for all these samples, indicating the presence of at least two sets of structures, one compact and one more extended. Early REMD simulations[33] suggest that the two ensembles populate the helix−coil and β-hairpin structure, respectively. However, the intensity ratios between the two peaks are quite different, indicating that the relative abundance of the compact and extended isoforms differ in these samples. For pure hIAPP, the compact to extended ratio is approximately 3:1. However, in both of the mixtures (hIAPP:insulin and hIAPP:IBC) the ratio increases to approximately 10:1, indicating a significant decrease in the extended isoform. We will come back to this point in the Conclusions section.

Molecular Modeling: Insight into the Details of the Amyloid Inhibition Process. The binding interaction between hIAPP and IBC was modeled from molecular dynamics (MD) simulations. The starting structures of +4 hIAPP include a β-sheet rich extended conformation and a helix-rich compact conformation, identified in our previous computational study[33] as well as in works by Reddy et al.[43] and Qiao et al.[44] A starting structure for the IBC was obtained from a long MD simulation (Figure S7 (SI)) initiated from the conformation extracted from the X-ray solved crystal structure of insulin (PDB id: 1GUJ). Note that an early NMR study has shown that isolated IBC adopts a helix-rich conformation in mixed aqueous organic solution, which is similar to its structure in intact insulin.[41]

IBC formed a complex with both hIAPP conformers in the last half of the simulations (see Figure S9 (SI)). The results based on the multiple snapshots within the last 100 ns of the binding simulations are summarized in Figure 6. The complex

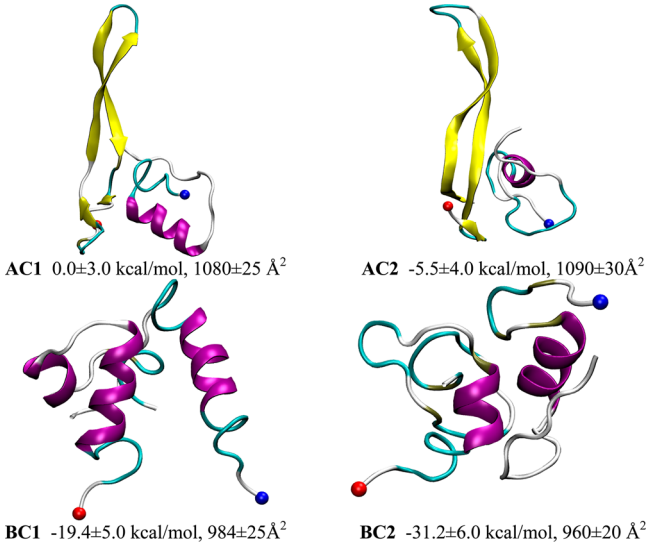

Figure 6. Representative snapshots of the four dimerization trajectories between +4 hIAPP and IBC. Whereas the N-terminus of +4 hIAPP is shown by a red ball, the N-terminus of IBC is shown by a blue ball. Collision cross section and the relative MM-GBSA binding energy between hIAPP and IBC with reference to the binding energy of the complex in AC1 are noted.

with the extended hairpin conformer of hIAPP (modeled as a hairpin−helix complex) has a calculated collision cross section of 1085 Å^2. In contrast, the complex with the helix-rich compact conformer of hIAPP (a helix−helix complex) has a calculated collision cross section of 972 Å^2. Thus, the helix−helix complex is 10% more compact than the helix-hairpin complex to the relative uncertainty of 1%. In addition MM-GBSA calculations indicate the helix−helix complex is significantly more stable than the hairpin−helix complex. When compared with the experimental data, the model

dx.doi.org/10.1021/ja504031d | J. Am. Chem. Soc. 2014, 136, 12912−12919

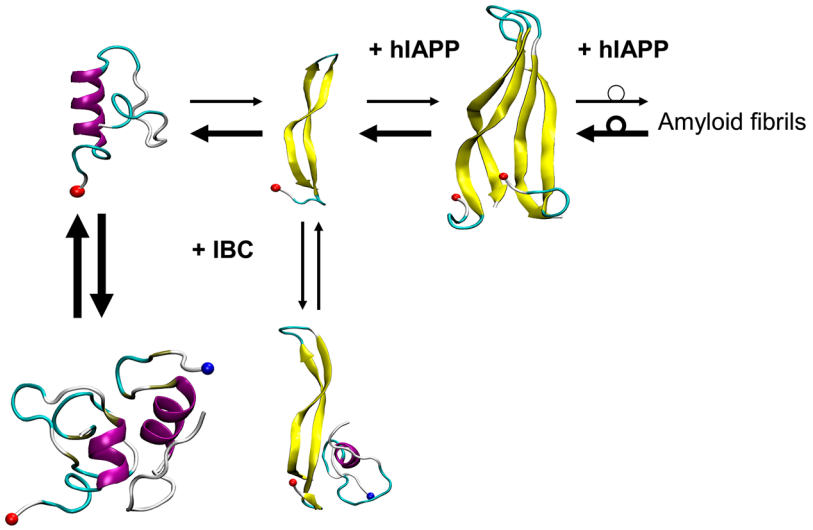

Figure 7. Proposed mechanism by which IBC inhibits hIAPP aggregation via predominantly forming helix/helix hIAPP:IBC complexes. The N-terminus of hIAPP and IBC is shown by a red and blue ball, respectively. Thick and thin arrows indicate, respectively, high and low reaction rates, leading to a reduction of the aggregation-prone β-hairpin of hIAPP. Residues 9−14 of hIAPP and 11−19 of IBC are located at the helix−helix interface (in purple color) of the most stable complex from the simulations (left-bottom).

helix−helix complex has a cross section 9% above the experimental cross section of 893 ± 9 Å^2, while the model hairpin−helix is 22% above the experimental value. Given the higher stability and the closer agreement with the experimental data, the helix−helix complex rather than the hairpin−helix complex appears to be the major stable species in the experiment. The larger value for the cross section from the calculation (∼9% for the helix−helix dimer) indicates that the actual packing between hIAPP and IBC is tighter than that found in the simulations. In order to get better agreement with experiment, higher level but computational expensive modeling, such as replica exchange methods would be needed. According to our modeling the major packing interface is between the helix (residues 9−18) of hIAPP and the helix (residues 11−19) of IBC leading to stronger van der Waals interactions than for the helix/β-hairpin interface. Of importance is the fact this interface is consistent with the peptide mapping results of Gazit and co-workers.[26] Interestingly, this interface is very similar to the binding interface between rIAPP and insulin, derived from a combined NMR and MD study by Wei et al.[31] This is not surprising, because both rIAPP and hIAPP can adopt similar transient helix-rich conformations and they have the almost same sequence in the N-terminal region (1−22) differing only by the H18R substitution.[28]

The binding between the two hIAPP conformers and the larger insulin monomer (PDB id: 1GUJ) was also modeled by MD simulations. A similar binding pattern to that of IBC and hIAPP was observed (Figure S11 (SI)). The insulin monomer formed a stable complex with both hIAPP monomer conformers and the major binding interaction was between the insulin B-chain (residues 11−19) and hIAPP (residues 8−18). This is consistent with our experimental observation that IBC monomer rather than IAC monomer plays an important role in interacting with hIAPP. In addition, the calculated binding energy of the insulin monomer to the helix-rich hIAPP conformer was significantly stronger than the calculated binding energy to the hairpin-rich hIAPP conformer based on our MM-GBSA binding calculations (Figure S11 (SI)). Hence, the results indicate that insulin forms stable complexes with either hIAPP conformer, but the binding to the helix-rich conformer is much stronger than to the hairpin-rich hIAPP conformer.

CONCLUSIONS

Insulin stabilizes hIAPP in a monomeric nonamyloidogenic state in solution at low molar ratios (1:1) for long periods of time. As long as insulin monomer is stable in solution, monomeric hIAPP is also stabilized through the formation of heterogeneous clusters of insulin and hIAPP. A single hIAPP monomer binds up to three insulin monomers, but no heterogeneous clusters are observed with more than one hIAPP monomer. Our IMS-MS study probes inhibition of the initial steps of hIAPP assembly. As such it does not exclude the interaction of insulin with larger hIAPP oligomers/profibrils, which also may have an inhibitory effect on later steps in hIAPP assembly. It is likely that insulin also interacts with larger hIAPP oligiomers as insulin inhibits hIAPP at substoichiometric concentrations.[20,25,29,45]

Like insulin, IBC monomers also stabilize hIAPP in a nonaggregating monomer state and form analogous heterogeneous clusters of one IBC monomer and one hIAPP monomer. However, IAC does not stabilize hIAPP monmers, and no heterogeneous clusters are observed in the mass spectrum of IAC/hIAPP mixtures. This indicates that the B-chain of insulin plays the primary role in stabilizing soluble hIAPP, which is consistent with our MD modeling and with the results of Gazit and co-workers.[26]

Ion mobility studies show that the extended structure of hIAPP is in much smaller abundance relative to the compact form of hIAPP monomer in the mixtures of hIAPP with insulin and insulin B chain compared to the pure hIAPP monomer. This suggests that insulin and IBC interact with hIAPP monomers, causing either the conversion of the extended conformation to the more compact structures or there is a depletion of the ensemble of extended conformations by binding to insulin. Our modeling, however is consistent with IBC and insulin forming significantly more stable complexes with the compact helix-rich conformer of hIAPP than with the extended β-hairpin structure. This result suggests insulin and

dx.doi.org/10.1021/ja504031d | J. Am. Chem. Soc. 2014, 136, 12912−12919

IBC monomers sequester hIAPP helix-rich monomers to form heterogeneous clusters and shift the equilibrium away from the extended monomer structure and toward the condensed α-helical monomer structure. A schematic view of this proposed mechanism is shown in Figure 7. The selective targeting of one set of conformations by insulin is similar to the effect of certain small molecule inhibitors of hIAPP that function by targeting one subset of the ensemble of hIAPP conformations,[46] suggesting that this may be a general strategy for inhibiting hIAPP amyloid formation.

Finally, our modeling results suggest the stabilization of the heterodimer complexes occur between residues 11 to 19 of IBC and 8 to 18 of hIAPP, a result consistent with the peptide mapping study of Gazit and co-workers.[26] Hence an excellent place to initiate a search for hIAPP aggregation inhibitors is in peptide fragments derived from the S^{9}HLVEALYLVCG^{20} segment of IBC. A related method has been fruitful in discovering inhibitors of soluble oligomer formation of Aβ42, and subsequently its toxicity. Aβ42 is the peptide primarily responsible for Alzheimer's disease.[47]

MATERIALS AND METHODS

A full description of the materials and methods is given in the Supporting Information. Briefly, the hIAPP samples used in this study were synthesized according to procedures previously described.[48,49] A hIAPP stock solution (1 mM) was prepared in hexafluoro-2-propanol (HFIP), and then aliquots of the stock were dried, and the peptides were resuspended in ammonium acetate buffer as previously described by Dupuis et al.[33,34] The bovine insulin (catalog no. I5500) as well as the separate A and B chains of bovine insulin were purchased from Sigma-Aldrich and used without further purification. Mass spectra were recorded on a prototype of the commercially available Synapt HDMS (Waters-Micromass, Manchester, U.K.) that features a nanoelectrospray ion source, an ion mobility cell and a high-resolution time-of-flight mass spectrometer.[50] To investigate the effects of insulin on the morphology of the insoluble aggregates from the samples, aliquots from the incubated samples were dried on freshly cleaved mica and imaged with an Asylum Research MFP-3D-SA atomic force microscope (Asylum Research, Santa Barbara, CA) following our early protocol.[33] Ion mobility measurements were recorded using a custom built instrument[51] with a nanoelectrospray ionization (ESI) source, ion funnel, ion mobility drift cell and quadrupole mass analyzer. The AMBER 8[52] simulation package was used in modeling the complexes formed by insulin and IBC with hIAPP. The AMBER all-atom point-charge protein force field, ff96[53] with an implicit solvent IGB = 5,[54] was used to model the peptides in this study. Recent accomplishments of this force field combination include both the successful *ab initio* folding of α, β, and α/β proteins[33,55−58] and the correct characterization of interdomain dynamics of a multidomain signal protein.[59] Multiple runs of the same experiment and simulation were conducted to obtain the uncertainty.

ASSOCIATED CONTENT

Supporting Information

Mass spectra for samples of insulin, hIAPP, IBC, IAC time course studies and molecular modeling data. Injection energy studies and isotopic spacing of the samples. This material is available free of charge via the Internet at http://pubs.acs.org.

AUTHOR INFORMATION

Corresponding Author

bowers@chem.ucsb.edu

Present Address

[§]Department of Chemistry and Biochemistry and Department of Biomedical and Translational Sciences, Rowan University, Glassboro, New Jersey 08028, United States.

Notes

The authors declare no competing financial interest.

ACKNOWLEDGMENTS

The support of the National Science Foundation Grants CHE-1301032 (MTB) and MCB-1158577 (JES) and National Institutes of Health Grant NIH-GM078114 (DPR) is gratefully acknowledged. M.T.B. also thanks Waters Corporation for donation of a Synapt prototype instrument used for part of the work presented here. J.E.S. also thanks David and Lucile Packard Foundation. The computation resources used the Extreme Science and Engineering Discovery Environment (XSEDE), which is supported by National Science Foundation Grant Number OCI-1053575, and the Center for Scientific Computing from the CNSI, MRL: an NSF MRSEC (DMR-1121053) and NSF CNS-0960316. The authors thank Nicholas Economou and Professor Steve Buratto at UCSB for helping with the AFM studies. The authors also thank Catie Carpenter for helping with the figures.

REFERENCES

(1) *National Diabetes Fact Sheet: National Estimates and General Information on Diabetes and Prediabetes in the United States*; Department of Health and Human Services, Centers for Disease Control and Prevention: Atlanta, GA, 2011.

(2) Janson, J.; Ashley, R. H.; Harrison, D.; McIntyre, S.; Butler, P. C. *Diabetes* **1999**, *48* (3), 491−498.

(3) Lin, C.-Y.; Gurlo, T.; Kayed, R.; Butler, A. E.; Haataja, L.; Glabe, C. G.; Butler, P. C. *Diabetes* **2007**, *56* (5), 1324−1332.

(4) Haataja, L.; Gurlo, T.; Huang, C. J.; Butler, P. C. *Endocr. Rev.* **2008**, *29* (3), 303−316.

(5) Huang, C. J.; Lin, C. Y.; Haataja, L.; Gurlo, T.; Butler, A. E.; Rizza, R. A.; Butler, P. C. *Diabetes* **2007**, *56* (8), 2016−2027.

(6) Laybutt, D. R.; Preston, A. M.; Akerfeldt, M. C.; Kench, J. G.; Busch, A. K.; Biankin, A. V.; Biden, T. J. *Diabetologia* **2007**, *50* (4), 752−763.

(7) Potter, K. J.; Abedini, A.; Marek, P.; Klimek, A. M.; Butterworth, S.; Driscoll, M.; Baker, R.; Nilsson, M. R.; Warnock, G. L.; Oberholzer, J.; Bertera, S.; Trucco, M.; Korbutt, G. S.; Fraser, P. E.; Raleigh, D. P.; Verchere, C. B. *Proc. Natl. Acad. Sci. U. S. A.* **2010**, *107* (9), 4305−4310.

(8) Westermark, G. T.; Westermark, P.; Berne, C.; Korsgren, O. *N. Engl. J. Med.* **2008**, *359* (9), 977−979.

(9) Udayasankar, J.; Kodama, K.; Hull, R. L.; Zraika, S.; Aston-Mourney, K.; Subramanian, S. L.; Tong, J.; Faulenbach, M. V.; Vidal, J.; Kahn, S. E. *Diabetologia* **2009**, *52* (1), 145−153.

(10) Westermark, P.; Andersson, A.; Westermark, G. T. *Physiol. Rev.* **2011**, *91* (3), 795−826.

(11) Cooper, G. J. S.; Aitken, J. F.; Zhang, S. *Diabetologia* **2010**, *53* (6), 1011−1016.

(12) Park, Y. J.; Lee, S.; Kieffer, T. J.; Warnock, G. L.; Safikhan, N.; Speck, M.; Hao, Z.; Woo, M.; Marzban, L. *Diabetologia* **2012**, *55* (4), 1035−1047.

(13) Brender, J. R.; Salamekh, S.; Ramamoorthy, A. *Acc. Chem. Res.* **2012**, *45* (3), 454−462.

(14) Cao, P.; Marek, P.; Noor, H.; Patsalo, V.; Tu, L. H.; Wang, H.; Abedini, A.; Raleigh, D. P. *FEBS Lett.* **2013**, *587* (8), 1106−1118.

(15) Young, A. A.; Vine, W.; Gedulin, B. R.; Pittner, R.; Janes, S.; Gaeta, L. S. L.; Percy, A.; Moore, C. X.; Koda, J. E.; Rink, T. J.; Beaumont, K. *Drug Dev. Res.* **1996**, *37* (4), 231−248.

(16) German, M. S.; Moss, L. G.; Wang, J. H.; Rutter, W. J. *Mol. Cell. Biol.* **1992**, *12* (4), 1777−1788.

(17) Hull, R. L.; Westermark, G. T.; Westermark, P.; Kahn, S. E. *J. Clin. Endocrinol. Metab.* **2004**, *89* (8), 3629−3643.
(18) Hutton, J. C. *Diabetologia* **1989**, *32* (5), 271−281.
(19) Smith, G. D.; Pangborn, W. A.; Blessing, R. H. *Acta Crystallogr., Sect. D: Biol. Crystallogr.* **2003**, *59*, 474−482.
(20) Knight, J. D.; Williamson, J. A.; Miranker, A. D. *Protein Sci.* **2008**, *17* (10), 1850−1856.
(21) Knight, J. D.; Miranker, A. D. *J. Mol. Biol.* **2004**, *341* (5), 1175−1187.
(22) Bram, Y.; Frydman-Marom, A.; Yanai, I.; Gilead, S.; Shaltiel-Karyo, R.; Amdursky, N.; Gazit, E. *Sci. Rep.* **2014**, *4*, 4267.
(23) Abedini, A.; Raleigh, D. P. *Biochemistry* **2005**, *44* (49), 16284−16291.
(24) Brender, J. R.; Hartman, K.; Nanga, R. P. R.; Popovych, N.; Bea, R. D.; Vivekanandan, S.; Marsh, E. N. G.; Ramamoorthy, A. *J. Am. Chem. Soc.* **2010**, *132* (26), 8973−8983.
(25) Cui, W.; Ma, J.-w.; Lei, P.; Wu, W.-h.; Yu, Y.-p.; Xiang, Y.; Tong, A.-j.; Zhao, Y.-f.; Li, Y.-m. *FEBS J.* **2009**, *276* (12), 3365−3371.
(26) Gilead, S.; Wolfenson, H.; Gazit, E. *Angew. Chem., Int. Ed.* **2006**, *45* (39), 6476−6480.
(27) Jaikaran, E. T. A. S.; Nilsson, M. R.; Clark, A. *Biochem. J.* **2004**, *377*, 709−716.
(28) Westermark, P.; Li, Z. C.; Westermark, G. T.; Leckstrom, A.; Steiner, D. F. *FEBS Lett.* **1996**, *379* (3), 203−206.
(29) Janciauskiene, S.; Eriksson, S.; Carlemalm, E.; Ahren, B. *Biochem. Biophys. Res. Commun.* **1997**, *236* (3), 580−585.
(30) Brender, J. R.; Lee, E. L.; Hartman, K.; Wong, P. T.; Ramamoorthy, A.; Steel, D. G.; Gafni, A. *Biophys. J.* **2011**, *100* (3), 685−692.
(31) Wei, L.; Jiang, P.; Yau, Y. H.; Summer, H.; Shochat, S. G.; Mu, Y. G.; Pervushin, K. *Biochemistry* **2009**, *48* (11), 2368−2376.
(32) Wiltzius, J.; Sievers, S.; Sawaya, M.; Eisenberg, D. *Protein Sci.* **2009**, *18* (7), 1521−1530.
(33) Dupuis, N. F.; Wu, C.; Shea, J. E.; Bowers, M. T. *J. Am. Chem. Soc.* **2009**, *131* (51), 18283−18292.
(34) Dupuis, N. F.; Wu, C.; Shea, J.-E.; Bowers, M. T. *J. Am. Chem. Soc.* **2011**, *133* (19), 7240−7243.
(35) Westermark, P.; Engstram, U.; Johnson, K. H.; Westermark, G. T.; Betsholtz, C. *Proc. Natl. Acad. Sci. U. S. A.* **1990**, *87* (13), 5036−5040.
(36) Butler, A. E.; Jang, J.; Gurlo, T.; Carty, M. D.; Soeller, W. C.; Butler, P. C. *Diabetes* **2004**, *53* (6), 1509−1516.
(37) Andreetto, E.; Yan, L.; Tatarek-Nossol, M.; Velkova, A.; Frank, R.; Kapurniotu, A. *Angew. Chem., Int. Ed.* **2010**, *49* (17), 3081−3085.
(38) Nettleton, E. J.; Tito, P.; Sunde, M.; Bouchard, M.; Dobson, C. M.; Robinson, C. V. *Biophys. J.* **2000**, *79* (2), 1053−1065.
(39) Ahmad, A.; Uversky, V. N.; Hong, D.; Fink, A. L. *J. Biol. Chem.* **2005**, *280* (52), 42669−42675.
(40) Goldsbury, C.; Goldie, K.; Pellaud, J.; Seelig, J.; Frey, P.; Muller, S. A.; Kistler, J.; Cooper, G. J. S.; Aebi, U. *J. Struct. Biol.* **2000**, *130* (2−3), 352−362.
(41) Hawkins, B.; Cross, K.; Craik, D. *Int. J. Pept. Protein Res.* **1995**, *46* (5), 424−433.
(42) Yonemoto, I. T.; Kroon, G. J. A.; Dyson, H. J.; Balch, W. E.; Kelly, J. W. *Biochemistry* **2008**, *47* (37), 9900−9910.
(43) Reddy, A. S.; Wang, L.; Singh, S.; Ling, Y.; Buchanan, L.; Zanni, M. T.; Skinner, J. L.; De Pablo, J. J. *Biophys. J.* **2010**, *99* (7), 2208−2216.
(44) Qiao, Q.; Bowman, G. R.; Huang, X. *J. Am. Chem. Soc.* **2013**, *135* (43), 16092−16101.
(45) Wang, H.; Raleigh, D. P. *Biochemistry* **2014**, *53* (16), 2605−2614.
(46) Young, L. M.; Cao, P.; Raleigh, D. P.; Ashcroft, A. E.; Radford, S. E. *J. Am. Chem. Soc.* **2014**, *136* (2), 660−670.
(47) Gessel, M. M.; Wu, C.; Li, H. Y.; Bitan, G.; Shea, J. E.; Bowers, M. T. *Biochemistry* **2012**, *51* (1), 108−117.
(48) Abedini, A.; Raleigh, D. P. *Org. Lett.* **2005**, *7* (4), 693−696.
(49) Abedini, A.; Singh, G.; Raleigh, D. P. *Anal. Biochem.* **2006**, *351* (2), 181−186.
(50) Pringle, S. D.; Giles, K.; Wildgoose, J. L.; Williams, J. P.; Slade, S. E.; Thalassinos, K.; Bateman, R. H.; Bowers, M. T.; Scrivens, J. H. *Int. J. Mass Spectrom.* **2007**, *261* (1), 1−12.
(51) Wyttenbach, T.; Kemper, P. R.; Bowers, M. T. *Int. J. Mass Spectrom.* **2001**, *212* (1−3), 13−23.
(52) Case, D. A.; Cheatham, T. E.; Darden, T.; Gohlke, H.; Luo, R.; Merz, K. M.; Onufriev, A.; Simmerling, C.; Wang, B.; Woods, R. J. *J. Comput. Chem.* **2005**, *26* (16), 1668−1688.
(53) Gunsteren, W. F. v.; Weiner, P. K.; Wilkinson, T. *Computer Simulation of Biomolecular Systems*; Kluwer Academic Publishers: Boston, 1997; p v.
(54) Onufriev, A.; Bashford, D.; Case, D. A. *Proteins: Struct. Funct., Bioinf.* **2004**, *55* (2), 383−394.
(55) Shell, M. S.; Ritterson, R.; Dill, K. A. *J. Phys. Chem. B* **2008**, *112* (22), 6878−6886.
(56) Voelz, V.; Bowman, G.; Beauchamp, K.; Pande, V. *J. Am. Chem. Soc.* **2010**, *132* (5), 1526−1528.
(57) Voelz, V.; Singh, V.; Wedemeyer, W.; Lapidus, L.; Pande, V. *J. Am. Chem. Soc.* **2010**, *132* (13), 4702−4709.
(58) Wu, C.; Shea, J. E. *PLoS Comput. Biol.* **2010**, *6* (11), e1000998.
(59) Wang, X. Q.; Wu, C.; Vu, A.; Shea, J. E.; Dahlquist, F. W. *J. Am. Chem. Soc.* **2012**, *134* (39), 16107−16110.